Development of Hole Conductivity of CuSCN by Adding Mn

H.M.K.L. HATHURUSINGHA[1], P.G.D.C.K. KARUNARATHNA[2], P. SAMARASEKARA[3]
[1, 3] *Department of Physics, University of Peradeniya, Peradeniya, Sri Lanka*
[2] *Department of Nano Science Technology, Wayamba University of Sri Lanka, Kuliyapitiya, Sri Lanka*

Abstract- ***Pure CuSCN thin films and Manganese doped CuSCN thin films were prepared using the doctor blade method. Electrical, optical, and structural properties of coated thin films were characterized. The variation of the electrical conductivity was investigated by using pure CuSCN samples and CuSCN samples with different Mn mass percentages. Mn mass percentage in CuSCN was varied from 2 to 10% in steps of 2%. The samples were subsequently annealed at 80 ^{0}C for 15 minutes. Structural and optical properties were characterized by means of XRD and UV visible spectrometer, respectively. According to the sheet resistance value for unit area of thin films, 6% Mn mass percentage added CuSCN sample exhibited the highest conductivity value, and conductivity gradually increased with Mn concentration in samples up to the doping concentration of 6%. According to the XRD data, crystalline size decreased with the doping of Mn. All the thin films exhibited absorbance and transmittance properties in the visible wavelength region. The calculated optical energy band gap of CuSCN is 3.18 eV. This produced Mn-doped CuSCN layer can be used as an efficient HTM layer in many applications.***

Indexed Terms- ***Copper thiocyanate, electrical conductivity, Manganese, optical band gap***

I. INTRODUCTION

Hole-transporting (p-type) materials that can be utilized as Hole injection, extraction, and transport interlayers in various optoelectronic devices and systems. They are used in various optoelectronic devices such as light-emitting diodes (LEDs), organic photovoltaics (OPV) and hybrid organic-inorganic photovoltaic cells [1]. Also, most intrinsic wide-bandgap semiconductors do not have an electronic or physical structure that can contribute to successful acceptor doping to generate excess mobile holes as the majority carriers. Optimum device performance requires high conductivity of those types of charge carriers. Because of limited supply of transparent and high-mobility p-type conductors, it shows a significant challenge to the advancement of optoelectronic technologies. Therefore, it is essential to identify p-type materials which are capable to meet the increasing demand for faster-operating frequencies and higher device efficiencies [2].

Copper thiocyanate (CuSCN) has received a significant attention as a Hole Transport Material (HTM) due to the higher maximum hole mobility of about 0.1 cm^2 V^{-1} s^{-1}. Moreover, CuSCN has suitable energy levels as well as affordable and simplified synthesis routes which make it suitable for applications [3]. Also recent advances in optoelectronics researches have reported that the huge potential of CuSCN as a universal hole-transport interlayer material for various applications, including transparent thin-film transistors, high-efficiency organic and hybrid organic-inorganic photovoltaic cells, and organic light-emitting diodes. CuSCN is also available from trade sources while it is inexpensive and can be processed at low-temperatures using solution-based methods [4]. These unique features and desirable characteristics make CuSCN a promising material for various applications. Therefore, CuSCN was selected as the starting material for this research to develop and investigate a HTM for applications. As already discussed earlier, CuSCN has been considered as a hole-transporting layer in numerous optoelectronic devices. However, the studies on the hole transport properties of CuSCN are very limited.
Even though CuSCN has widespread use as a hole-transporting layer in various optoelectronic devices, only the charge carrier transport mechanisms in CuSCN have been studied. In 2017, Neeraj Chaudhary et al. reported the solution processed CuSCN thin film

deposition for organic solar cells, researchers used the environmentally friendly and inexpensive solvent dimethyl sulfoxide (DMSO) [5]. By investigating the temperature dependency of the field-effect hole mobility of CuSCN based thin-film transistors, three different transport designs were identified for solution-processed CuSCN layers. At high temperatures (228 K–303 K), the transport was highly thermal activated, a signature of the Multiple Trapping and Release (MTR) the mode which is an archetype model for transport in nanocrystalline in organic semiconductors. In this case, carriers can still travel as waves in the extended states outside the mobility gap but become momentarily trapped by the localized states in the band tail before being released via thermal activation. At intermediate temperatures (123 K–228 K), the transport mechanism was also thermally activated but with a smaller energy barrier. Based on similar observations in nanocrystalline inorganic semiconductors, the transport process followed the Variable Range Hopping (VRH) mechanism in this temperature range [6].

Previous theoretical works mainly employ the density functional theory (DFT) calculations to explain the electronic structure of the most popular form of CuSCN, the hexagonal β-CuSCN. The results of the valence band (VB) and conduction band (CB) structures of different studies are similar to each other. Near the band edges of CuSCN, there are two significant characteristics: (1) the strong Cu 3d character near the VB edge, with some hybridization from the sp^3 states, and (2) the antibonding π^* character associated with the cyanide portion near the CB edge. These properties lead to good hole transport and the expected large indirect bandgap, both these result in the dominant p-type characteristics and the extremely high transparency in the visible range. When CuSCN has been used as a replacement for the commonly used poly(3,4-ethylenedioxythiophene): polystyrenesulfonate (PEDOT: PSS) [7]. In 2005, Hehl et al. reported that CuSCN is a unique semiconductor material since thin films free of defects and pinholes can be deposited on large surface areas due to its polymer-like structure. Polyanionic networks on the basis of thiocyanatometallates of Cu1 and Ag1 led to the synthesis of three new tris(thiocyanato)dimetallates(I) A[M2(SCN)3] with M = Cu, Ag and A = Me3NH and A = [Me2CNMe2] has been built up [8]. The p-type CuSCN has been studied mainly for use as a hole-transporting layer for photovoltaic applications. TiO_2 porous layer based Iodine/Iodide free dye sensitized solar cells have been fabricated [9]. In 2017, Anna Regoutz et al. reported that Spin casting, ink-jet printing, doctor blading, spray coating, and electrochemical deposition are only a few of the solution-processing methods that can deposit CuSCN at low temperatures [4].

CuSCN electrodeposition performed in organic solvents like Sulphur base solvents (diisopropyl sulfide and diethyl sulfide) was reported, Polymer solar cells with CuSCN nanowires as a new hole transporting material has been reported [10]. In 2004, V.P.S. Perera et al. have discovered that halogen gases that can generate extra SCN in a solution and can increase the conductivity of pure CuSCN. In this method, glass plates were placed on a hot plate (70–80^0C) and the solution was lightly spread on the surface with a dropper. The time variations of the two-probe sheet resistance of the films were determined with a Keithley multimeter after thin films were placed in a container filled with N_2 and small amounts of Iodine [11]. In 2018, S Samarakoon et al. fabricated Fe doped CuSCN layer using $FeSO_4$. p-CuSCN doped with Fe was used for the first time in this study to improve the light absorption properties. The development of a p-n junction is used to improve efficiency by providing efficient charge separation. In that low cost method, Cu_2S was used to form the p-n junction with Fe doped CuSCN [12]. Wide band gap materials such as ZnO are vastly used in photovoltaic applications [13].

In this manuscript, properties of Mn doped CuSCN thin film samples fabricated using the doctor blade method is explained. Structural, optical and electrical properties of these thin films were investigated. Variation of the electrical conductivity with the doping concentration was investigated by measuring the sheet resistance of the samples. The conductivity of p-type CuSCN could be enhanced by doping Mn. Because holes mainly contribute to the conductivity of p-type materials, this can be considered as a development of hole conductivity of CuSCN.

II. EXPERIMENTAL

First the mortar and pestle set, spatulas, and weighing boats were cleaned properly using ethanol and were dried up. Then 1250 mg of CuSCN powder was measured using the digital balance and added to the mortar. The powder was ground properly using a pestle to get finely dusted powder. Then 5 ml of dimethyl sulfoxide (DMSO) solution was measured by using a well cleaned 5 ml pipette. Thereafter, the solution and the prepared powder were added to a beaker and mixed them well. The solution was stirred for 1 hour to get a properly mixed sample using a magnetic stirrer. After that, the sample contained beaker was placed in an ultrasonic bath sonicator for 2 hours at room temperature to convert large particles to the fine particles. To avoid the temperature increase of the sonicator with time, the sonicator was switched off to cool down at each 15 min time intervals.

To prepare Mn added CuSCN samples, 25, 50, 75, 100 and 125 mg of $MnSO_4$ powder were added to 1250 mg of CuCSN sample to make CuSCN: Mn mass ratio as 2%, 4%, 6%, 8%, and 10%, respectively. For each $MnSO_4$ sample, 5 drops of distilled water were added and mixed well. After that, 1250 mg of CuSCN sample was placed in a motor and ground to prepare a fine powder using a pestle. Then previously prepared one $MnSO_4$ sample was added to the same motor. Thereafter, two samples were ground together for nearly one hour to get a well-mixed powder sample. The same procedure was followed for all the other prepared CuSCN:$MnSO_4$ mixtures. Prepared powder-like products were placed in separate beakers and labeled for identification. After that, 5 ml of DMSO samples were added to each container using a pipette. Finally each mixture was mixed on a magnetic stirrer for 1 hour and sonicated in an ultrasound bath for 2 hours at room temperature.

Thin film samples were prepared on borosilicate amorphous glass substrates and conductive glass substrates. The glass substrates were cleaned as follows. Glass slides were cut into 2 cm x 1.5 cm pieces using a glass cutter. Glass substrates were first cleaned using detergent and water, and then using DI water for further cleaning. Those glass plates were immersed in a beaker containing 30% concentrated HCl solution and sonicated for 30 mins. Next those plates were immersed again in a beaker containing deionized water and sonicated for 30 min. After that each glass substrate was dried well using a drier. The cleaned glass plates were placed on a piece of furnace tile by keeping enough distance between plates. Then those glass plates were attached to the tile using glue tapes. Both sides were covered by tapes in order to obtain thin films with the same thickness. Then thin films were synthesized using the Doctor blade method. Then prepared thin films were kept at room temperature for 15 mins and attached tapes were removed after 15 minutes. Then thin films were annealed at 80 ^{0}C in a furnace for 15 minutes.

X-ray diffraction (XRD) patterns of all the samples were measured using a Bruker D8 Advanced Eco Powder X-ray Diffraction system was used to analyze the samples. And the Cu-Ka (λ =1.5406 ^{0}A) radiation. The sheet resistance of the samples was measured using a universal Four Point Probe with RM3000 Test Unit. Optical band gap was measured by means of a Double Beam UV-visible spectrometer (UV-1800 Shimadzu) at room temperature. Impedance measurements were performed using a Keithley 6400 sourcemeter AUTOLAB. Samples prepared on borosilicate glass substrates were used for XRD, FTIR and UV-visible spectroscopies. Samples synthesized on conductive glass substrates were used for sheet resistance and impedance measurements.

III. RESULTS AND DISCUSSION

Fig. 1 and 2 show the XRD pattern of pure CuSCN and 10% Mn doped CuSCN thin films, respectively. The peak positions for CuSCN powder were determined using the International Center of Diffraction Data card ICDD; formerly JCPDS,29-0582). The characteristic peaks due to reflection from the planes (020), (120), (121), (200), (211), (112), (140), (141), and (132) are the same as the JCPDS peaks. Any additional peaks corresponding to the formation of mixed oxides were not observed. The doping of manganese does not provide additional peaks in the crystalline structure of pure CuSCN, and doping only changes the peak positions and intensity of some peaks slightly. The XRD data reveals that Mn is properly doped.

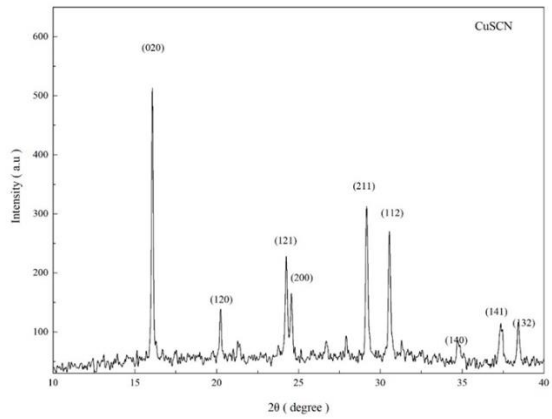

Fig. 1: XRD pattern for pure CuSCN thin film.

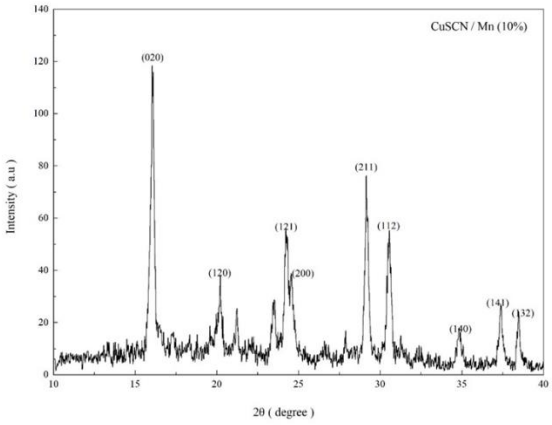

Fig. 2: XRD pattern for 10%Mn added CuSCN thin film.

The mean Crystalline size (D) of these particles was determined using Scherrer's approximation,

$$D = \frac{0.91\lambda}{\beta \cos\theta}$$

Where λ is the wavelength of Cu-Kα radiation (λ =1.5406 ^{0}A) and β is the full width at half maximum (FWHM) of XRD peak at angle θ. Crystallite sizes of pure CuSCN and Mn doped CuSCN are given in Table I. Crystalline sizes decrease with the added dopants, because the ionic radius of the Mn^{+2} (70 pm) is small than the Cu^{+1} (77 pm) radius. These calculations were done for (020) plane with the maximum intensity.

Table I: Values of FWHM, θ, and crystalline sizes for pure and 10% Mn doped CuSCN thin films.

Doping Concentration	Maximum intensity angle (θ) (Rad)	Full width at half maximum (FWHM)	Crystalline size (nm)
Pure CuSCN	8.03428	0.11466	70.79
10% Mn	8.02774	0.28686	28.32

Fig. 3 shows the UV-visible absorption spectrum of the pure CuSCN thin film. According to figure, the pure CuSCN has lower absorbance values in the visible region. The band gap of pure CuSCN sample was calculated using the intercept of the tangential line drawn to the curve. The band gap was found to be 3.18 eV, which is approximately equal to the standard value of the band gap of pure CuSCN.

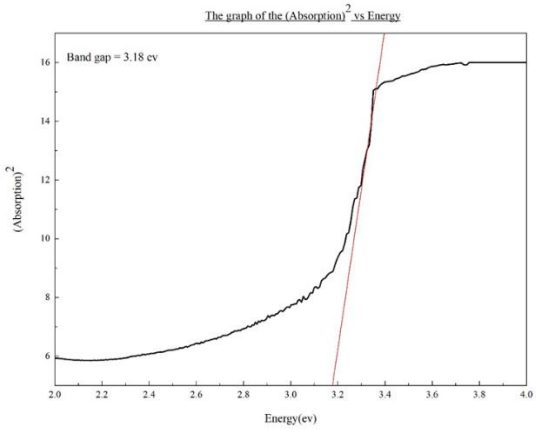

Fig. 3: Graph of $(Absorption)^2$ vs Energy for pure CuSCN thin film.

Table II shows the sheet resistance values of thin films with different doping concentrations. Fig. 4 shows the graph of sheet resistance versus Mn doping concentration. The highest conductivity was found at 6% of Mn doping concentration. The conductivity of manganese doped CuSCN increases mainly due to the increase of defect concentration from manganese. When the manganese concentration is higher, the defect concentration also will be higher. Addition of extra energy levels due to the doping causes to the decrease of the band gap. When the band gap decreases, the concentration of free charge carriers such as electrons and holes increase. As a result, the electrical conductivity enhances. Above the doping concentration of 6%, the conductivity decreases. The higher the dopant concentration is the higher the

probability that dopant ions take place on the grain boundaries. In addition, the scattering of conduction charge carriers increases because the field inside the crystal is fluctuated due to the existence of high concentration of impurity atoms. As a result, the conductivity decreases.

Table II: Sheet resistance of samples with different doping concentrations.

Doping Concentration (Weight ratio)	Sheet Resistance Ωm^{-2}
Pure CuSCN	1098
2% Mn	1042
4% Mn	95
6% Mn	31
8% Mn	183

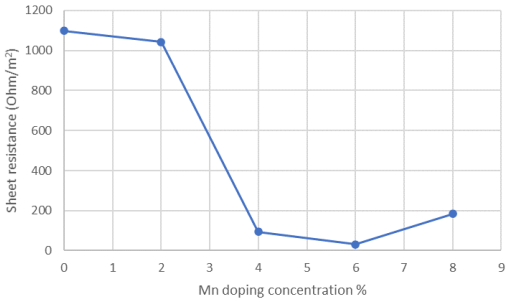

Fig. 4: Sheet resistance of sample versus Mn doping concentration.

Fig. 5 represents the graph of electric current versus applied potential for 6% Mn doped (solid line) and pure CuSCN (dotted line) samples. This graph verifies that the 6% Mn doped sample has a higher conductivity compared to the pure CuSCN sample. Slopes of the straight lines of pure and 6% Mn doped samples are $6.46x10^5$ and $2.15x10^6$ A V^{-1}, respectively.

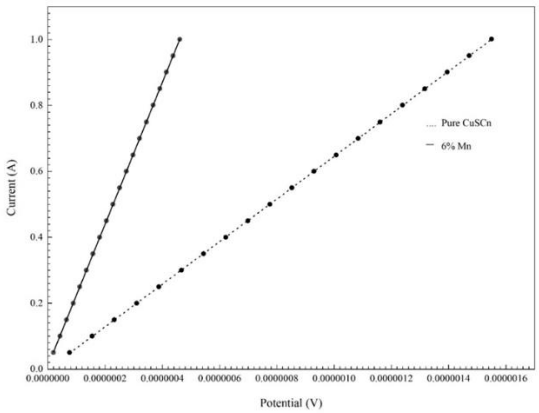

Fig. 5: I-V curves of pure CuSCN and 6% Mn doped sample.

Fig. 6 shows the Nyquist plots of the pure CuSCN (dotted line) and 6% Mn doped (solid line) samples. Because the plot consists of a semicircle and a straight line, it is equivalent to a full Randle circuit with two resistors, capacitor and Warburg impedance. Polarization resistance values estimated for 6% Mn doped CuSCN and pure CuSCN samples were found to be 600000 and 2350000 Ω, respectively. These curves confirm that 6% Mn doped sample has a lower conductivity compared to the pure CuSCN sample. Both the real and imaginary parts of the impedance of pure CuSCN sample are higher compared to those of the 6% doped sample.

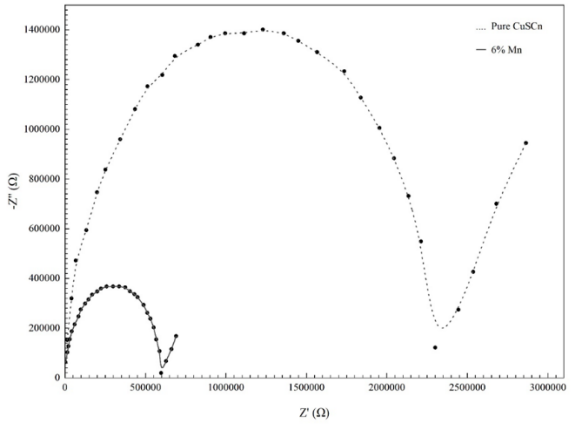

Fig. 6: Nyquist plots of the pure CuSCN and 6% Mn doped samples.

Fig. 7 represents the Bode plots of the pure CuSCN (dotted line) and 6% Mn doped (solid line) samples. This curves confirm that the impedance of pure CuSCN sample is higher than that of 6% Mn doped

sample. Adding Mn enhances the conductivity of many compounds [14] - [18]. Some studies have revealed that Mn ions with unpaired electrons decrease the dielectric constant value of the sample, and hence causing to enhance in conductivity of the system due to the increase of number of mobile charge carriers [14]. In addition, the conductivity of Mn doped sample increases due to the Schottky emission [15]. After doping with Mn, the 4d orbital of the Mn atom will have five electrons. Therefore, it is easier to lose a single electron from the outer subshell of the 4d orbital [16]. Doping Mn can enhance the hole carrier concentration and carrier mobility [17]. Furthermore, Mn doping can improve the densification of the material [18].

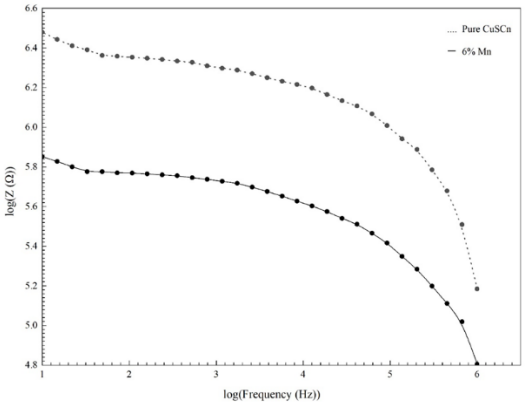

Fig. 7: Bode plots of the pure CuSCN and 6% Mn doped samples.

Fig. 8 represents the Bode phase diagrams of the pure CuSCN (dotted line) and 6% Mn doped (solid line) samples. Overlapping of two curves implies that the life time of the electrons does not change due to the doping. According to these curves, both samples act as high band pass filters.

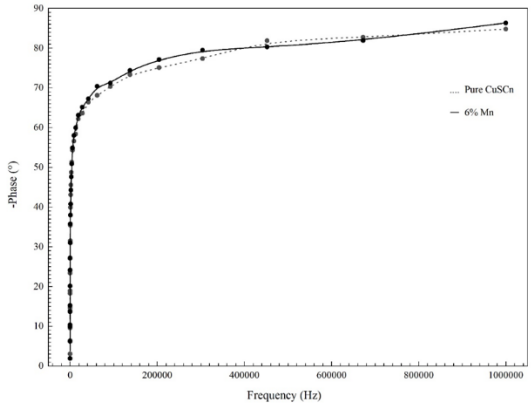

Fig. 8: Bode phase diagrams of the pure CuSCN and 6% Mn doped samples.

CONCLUSION

XRD patterns of the samples indicate the formation of CuSCN in thin film form. The doping of Mn up to 10% does not change the XRD patterns. The sheet resistance data, I-V curves, Nyquist plots, Bode plots and Bode phase diagrams confirm that the 6% Mn doped sample has a higher electrical conductivity compared to pure CuSCN. The electrical conductivity enhances with doping due to the addition of impurity energy levels, which reduces the optical band gap. Crystalline size decreases due to the doping of Mn, because the ionic radius of the Mn^{+2} is small than that of Cu^{+1}. Doping 10% of Mn decrease the crystalline size of pure CuSCN by 40%. The sheet resistance of 6% Mn doped sample is only 8.65% of pure CuSCN sample. The decrease of crystalline size increases the effective surface area, which can be attributed to the enhancement of the electrical conductivity.

REFERENCES

[1] N. Wijeyasinghe, and T. Anthopoulos, - Topical Review: Copper (I) thiocyanate (CuSCN) as a hole-transport material for large-area opto/electronics, ‖ *Semiconductor Science and Technology*, vol. 30, article ID. 104002, Oct. 2015.

[2] H. Ohta, K. Nomura, H. Hiramatsu, K. Ueda, T. Kamiya, M. Hirano and H. Hosono, - Frontier of transparent oxide semiconductors, ‖ *Solid-State Electronics*, vol. 47, pp. 2261- 2267, Dec. 2003.

[3] F. Matebese, R. Taziwa and D. Mutukwa, - Progress on the synthesis and application of

CuSCN inorganic hole transport material in perovskite solar cells, ‖ *Materials*, vol. 11, article ID. 2592, Nov. 2018.

[4] P. Pattanasattayavong, V. Promarak and T. Anthopoulos, - Electronic properties of copper (I) thiocyanate (CuSCN), ‖ *Advanced Electronic Materials*, vol. 3, article ID. 1600378, Feb. 2017.

[5] N. Chaudhary, R. Chaudhary, J. Kesari and A. Patra, - An eco-friendly and inexpensive solvent for solution processable CuSCN as a hole transporting layer in organic solar cells. ‖ *Optical Materials*, vol. 69, pp. 367-371, July 2017.

[6] P. Pattanasattayavong, A.D. Mottram, F. Yan and T. Anthopoulos, - Study of the hole-transport processes in solution-processed layers of the wide-bandgap semiconductor copper (I) Thiocyanate (CuSCN),‖ *Advanced Functional Materials*, vol. 25, pp. 6802-6813, Oct. 2015.

[7] N. Yaacobi-Gross, N. Treat, P. Pattanasattayavong, H. Faber, A. Perumal, N. Stingelin, D. Bradley, P. Stavrinou, M. Heeney and T. Anthopoulos, - High efficiency organic photovoltaic cells based on the solution processable hole transporting interlayer copper thiocyanate (CuSCN) as a replacement for PEDOT:PSS, ‖ *Advanced Energy Materials*, vol. 5, article ID. 1401529, Sept. 2014.

[8] R. Hehl and G. Thiele, - Synthesis and crystal structure of Me3NHCu2(SCN)3, Me2C=NMe2Cu2(SCN)3, and Me2C=NMe2Ag(SCN)3, Three dimensional networks of thiocyanatometallates(I), ‖ *Zeitschrift Für Anorganische Und Allgemeine Chemie*, vol. 626, pp. 2167-2172, Oct. 2000.

[9] S. Yanagida, Y. Yu and K. Manseki, - Iodine/Iodide-Free Dye-Sensitized Solar Cells, ‖ *Accounts of Chemical Research*, vol. 42(11), pp.1827-1838, March 2009.

[10] C. Chappaz-Gillot, S. Berson, R. Salazar, B. Lechêne, D. Aldakov, V. Delaye, S. Guillerez and V. Ivanova, - Polymer solar cells with electrodeposited CuSCN nanowires as new efficient hole transporting layer, ‖ *Solar Energy Materials and Solar Cells*, vol. 120, pp. 163-167, January 2014.

[11] V. Perera, M. Senevirathna, P. Pitigala and K. Tennakone, - Doping CuSCN films for enhancement of conductivity: Application in dye-sensitized solid-state solar cells, ‖ *Solar Energy Materials and Solar Cells*, vol. 86, pp. 443-450, March 2005.

[12] S. Samarakoon, P. Karunarathna and C. Fernando, - Characterization of Fe doped n-CuSCN/p-Cu_2S solid state photovoltaic cell, ‖ *Materials Research Express*, vol. 5, article ID 065052, June 2018.

[13] P. Samarasekara, A.G.K. Nisantha and A.S. Disanayake, - High Photo-Voltage Zinc Oxide Thin Films Deposited by DC Sputtering, ‖ *Chinese Journal of Physics*, vol. 40(2**)**, pp. 196-199, Apr. 2002.

[14] K.M. Sangwan, N. Ahlawat, S. Rani, S. Rani and R.S. Kundu, – Influence of Mn doping on electrical conductivity of lead free BaZrTiO3 perovskite ceramic, ‖ *Ceramics international*, vol. 44(9), pp. 10315-10321, June 2018.

[15] A. Semenov, A. Dedyk, I. Mylnikov, O, Pakhomov, A. Es'kov, A. Anokhin, V. Krylov, A. Burovikhin, Y. Pavlova, A. Tselev and A. Kholkin, - Mn- doped BaTiO3 Ceramics: Thermal and electrical properties for multicaloric applications, ‖ *Materials*, vol. 12, article ID 3592, Oct. 2019.

[16] J. Zou, L. Wang, J. He, B. Wu and Q. Xie, - Effects of Fe, Mn individual doping and (Fe, Mn) Co doping on ferromagnetic properties of Co_2Si powders, ‖ *Nanomaterials*, vol. 12(2), article ID 293, Jan. 2022.

[17] F.S. Liu, J.X. Zheng, M.J. Huang, L.P. He, W.Q. Ao, F. Pan and J.Q. Li, - Enhanced thermoelectric performance of Cu2CdSnSe4 by Mn doping: experimental and first principle studies, ‖ *Scientific Reports*, vol. 4, article ID 5774, July 2014.

[18] E.L. Santos, R. Muccillo and E.N.S. Muccillo, - Densification and electrical conductivity of Mn doped CeO_2, ‖ *Materials Science Forum*, vol. 591-593, pp. 639-643, Aug. 2008.